ELSEVIER

Biomaterials 19 (1998) 455–464

Biomaterials

Auger electron spectroscopy and its use for the characterization of titanium and hydroxyapatite surfaces

J.L. Ong[a,*], L.C. Lucas[b]

[a] University of Texas Health Science Center at San Antonio, Department of Restorative Dentistry, Division of Biomaterials, 7703 Floyd Curl Drive, San Antonio, TX 78284-7890, USA

[b] University of Alabama at Birmingham, Department of Biomedical Engineering, 256 Business-Engineering Complex, 1150 Tenth Avenue South, Birmingham, AL 35294-4461, USA

Received 1 September 1996; accepted 1 February 1997

Abstract

This review paper provides the basic background and underlying theory behind Auger electron spectroscopy (AES). Among the many surface analytical tools, AES has been shown to be very effective for surface composition analysis. These analyses are critically needed to better understand the interactions between the host and implant. The use of AES for titanium (Ti) and hydroxyapatite (HA) biomaterials characterization is demonstrated in this paper. The relative peak heights of $TiL_{2,3}M_{2,3}V$ can be used as 'fingerprints' for TiO_2 surfaces which have undergone different degrees of reduction. Similarly, for HA coatings, a shift in the phosphorus Auger peaks to a higher kinetic energy indicates the presence of a phosphate group, with strong P–O bonds.

Depth compositional profiling and thin-film analysis can be performed using AES. In our studies, oxide thicknesses on Ti surfaces range from 36.8 ± 7.4 Å to 436 ± 49 Å depending on the surface treatment. Depth profiling can also be used to determine the subsurface composition of biomaterials. For HA coatings, a phosphorus concentration at the oxide/metal interface has been observed to be higher than at the outermost oxide surface. The HA coatings have also been observed to coexist within the titanium oxide, suggesting the occurrence of chemical bonding between the coatings and the metallic substrates.

However, like other analytical tools, AES has its limitations. The electron beam damage can severely limit useful analysis of organic and biological materials and occasionally ceramic materials. Carbide buildup during long beam exposure times has been shown to affect the relative peak-to-peak intensities of the oxygen and metal Auger signals. The determination of film thickness requires a standard of known thickness and depth profiling of overlapping peaks can be very problematic. Even with these limitation, AES can be a powerful analytical tool for the characterization of biomaterial surfaces.

Keywords: Auger electron spectroscopy; Titanium; Hydroxyapatite; Depth profiling; Surface composition

1. Introduction

Although bulk properties dictate the mechanical properties of biomaterials, tissue–biomaterials interactions are a surface phenomena and are governed by surface properties. These interactions have been hypothesized to occur within a narrow zone of <1 nm [1]. Often, modification of biomaterials surfaces are employed as a mean of controlling tissue–biomaterials interactions. Surface modification for implant surfaces include passivation, anodization, coatings and different sterilization techniques. Radio-frequency glow-discharge treatments have been used to produce clean, surface-activated surfaces, with thinner and more stable oxide films [2–4]. Compared to acid passivation, sterilization of titanium (Ti) using either ethylene oxide gas or ethyl alcohol immersion has been reported to exhibit signification reductions in fibroblast attachment, with no significant spreading [5]. Conventional sterilization of Ti has compromised the surface properties by depositing organic contaminants on the surfaces, thereby affecting the fibroblast attachment. Inhibition of cell attachment on steam autoclaved Ti surfaces has also been reported [5, 6]. Studies have also investigated the attachment of polyethylene glycol as means of inhibiting bacterial growth [7, 8].

* Corresponding author.

0142-9612/98/$19.00
PII S0142-9612(97)00224-X

The initial interaction between the host and implant involves the conditioning of implants by serum and other tissue fluids, thereby resulting in compositional changes at the biomaterial surface [9–14]. Incorporation of carbonates and sodium from the biological environment into the calcium phosphate or hydroxyapatite (HA) coatings has been reported to increase the dissolution rate of coatings [15–17]. Spontaneous reprecipitation has been observed to depend on environmental pH, temperature, ionic concentrations, calcium/phosphorus (Ca/P) molar ratio and presence of organic or inorganic elements [18]. Organic phosphates and phosphonates are well known to have high affinities for adsorption to apatitic surfaces [19, 20]. As a result of dissolution/reprecipitation processes at the biomaterials surface, a dynamic change in surface composition is often observed. This dynamic surface becomes critical for intermediaries such as protein adsorption required for the stimulation of tissue responses [17, 21].

Thus, surface characterization of biomaterials is of prime importance for the functionality and behavior of tissues/cells at the biomaterials-tissue interface [22–26]. Surface characterization is often required to elucidate tissue/cellular behavior at the biomaterials–tissue interface. Modern spectroscopic surface analyses provide information on elemental composition, chemical state, and functional groups [27]. The objective of this paper is to present an overall view of Auger electron spectroscopy (AES) and its use in the characterization of Ti and sputtered HA coatings.

2. Background and theory of AES

One of the commonly used spectroscopy techniques for metallic and ceramic biomaterials is AES. Although the technique of electron-excited AES was reported in the mid fifties by Lander, it did not become widely used as a surface tool for more than a decade [28]. The reason for this delay was largely due to experimental difficulty in retrieving the characteristic Auger features from the large background of inelastically scattered electrons. In 1968, AES was generally accepted after Harris demonstrated that the characteristics of AES structures could be simply retrieved by differentiating the electron spectrum with respect to energy [29, 30]. These reports enabled AES to be used for obtaining critical chemical information on the biomaterials surface and subsurface.

The use of AES involves precise measurements of a number of emitted secondary electrons as a function of kinetic energy. When incident radiation, such as photons, electrons, ions, or neutral atoms, interacts with an atom that has an energy exceeding that necessary to remove an inner-shell electron from the atom, Auger electrons are produced. This interaction leaves the atom in an excited state with a core hole or a missing inner-shell electron

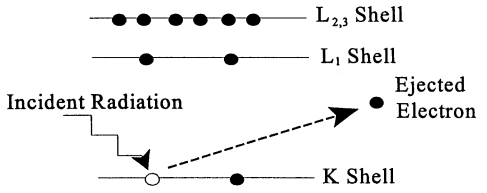

Fig. 1. Schematic showing the irradiation of the KLL shell. The interaction leaves the atom in an excited state with a core hole or a missing inner-shell electron.

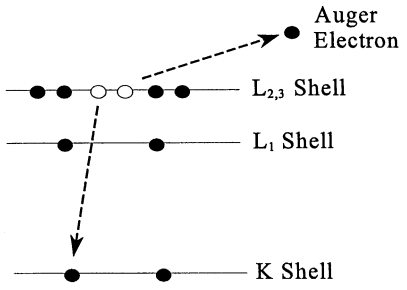

Fig. 2. Schematic showing the immediate de-excitation of the excited atom, resulting in the emission of an X-ray or Auger electron.

(Fig. 1). These excited atoms are unstable, and de-excitation occurs immediately, resulting in the emission of an X-ray or an electron defined as an Auger electron (Fig. 2). Fig. 2 shows the emission of a specific Auger electron via a $KL_{2,3}L_{2,3}$ transition. Since most atoms have several electron shells and subshells, it is possible for the emission of other electrons. All elements, except hydrogen and helium, produce high Auger yields, making AES highly sensitive for light element detection on the surface or subsurface (0–3 nm region). AES is also used for depth profiling, surface mapping, and thin film analysis [31, 32]. Chemical composition at the grain boundary is known to play an important role in such phenomena as high-temperature stress rupture strength and microfissuring in heat-affected zones of welds. Thus, in situ grain-boundary and other interfacial analyses facilitated by fracture are routinely conducted using AES [33].

2.1. Instrumentation

Analyses using AES require the sample to be inserted into an ultra high vacuum (UHV), usually at a base pressure of 10^{-7} Pa or less. To achieve an UHV, it is normal to bake the internal volumes in the AES system such as the chambers and pipework. During this bake-out treatment, the outgassing rate is temporarily increased so that the internally adsorbed gas is driven off and then pumped away. On return to room temperature, the outgassing rate will drop and the pumps can then produce and maintain an UHV. Bake out is controlled automatically and is normally conducted overnight.

As previously mentioned, the only function of the incident electron beam in AES is the ionization of core

levels to initiate the Auger process. Thus, it is critical that the energy in the electron beam is high enough to ionize all core levels of interest with high and uniform efficiency. Two types of electron sources are used in AES, thermionic and field emission. The more commonly used thermionic emission source requires that a material be heated to a temperature high enough for electrons to have energy sufficiently greater than the work function barrier. The electrons can then escape from the material's surface into the vacuum. The field emission source, also known as the 'high brightness' source, operates by reduction of the height of the work function barrier through application of a high electrostatic field. Thus, at room temperature, electrons can escape from the material into the vacuum. The emitting area of a field emission source is small and the emission is concentrated in a small solid angle, thereby allowing a higher current density per unit solid angle compared to a thermionic source.

Analysis of an AES electron energy spectrum is performed by an electrostatic electron energy analyzer. There are many different types of electrostatic analyzers such as the retarding field analyzers (RFA), the concentric hemispherical analyzers (CHA) and the cylindrical mirror analyzers (CMA). The RFA has been important in the development of the AES [34]. However, it is inherently unsuitable for general applications and has not been used in AES because of its poor signal-to-noise characteristics. The CHA, also known as the spherical sector analyzer or the spherical deflection analyzer, is used in X-ray photoelectron spectroscopy [35, 36]. The CMA is more suitable for AES due to its very high solid angle of acceptance which leads to high transmission [37]. The source area of Auger electrons is nearly always smaller than the acceptance area of the analyzer. Thus, high transmission from a small source area generally leads to optimization of the signal-to-noise ratio in AES. Disadvantages in the operation of the CMA is the sensitivity to sample position which could cause a drop in signal intensity, and a shift in peak energy if the sample is removed from the correct focal position [37].

2.2. Data acquisition

During data acquisition, the electron energy distribution, $N(E)$, plots contain direct information of Auger transitions. An example of the direct $N(E)$ spectrum is shown in Fig. 3. The Auger electron signal is related to the area under the appropriate peak in the direct $N(E)$ spectrum. The differential mode, $dN(E)/dE$ function, which reduces the effect of a high background, can be generated by electronic or digital conversion methods. A differentiated spectrum of a nickel–chromium–beryllium dental alloy surface is shown in Fig. 4. Historically, the differential mode has been used when the Auger electron peaks are small and, in the direct spectrum, may be superimposed on a sloping background. This electronic method of generating dN/dE involves superimposition of a small alternating current voltage on the outer cylinder and synchronous detection of the in-phase component of the analyzer output using a lock-in amplifier. Measurement of a differential energy spectrum usually involves the peak-to-peak value of the signal. This method of measurement is usually valid if the peak shapes are the same in the analysis and reference spectra, if the resolution of the analyzers used are the same for both spectra, and if the same modulation or differentiating algorithm is used [38]. This method of measurement is also based on the assumption that the shapes of Auger features do not change with the conditions of the experiment (such as surface chemistry). However, studies have demonstrated that the distortion in the shape of Ti and titanium oxide spectra do occur, and as a result, the peak-to-peak signals give erroneous relative values [39, 40]. Grant et al. reported that the magnitude and shape of Auger spectra are better behaved as a function of the modulation amplitude, and that enormous

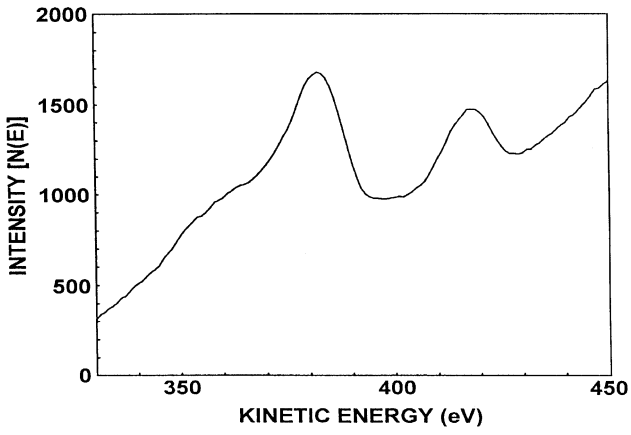

Fig. 3. Example of an AES spectrum showing a direct electron energy distribution, $N(E)$, plot of Ti LMM.

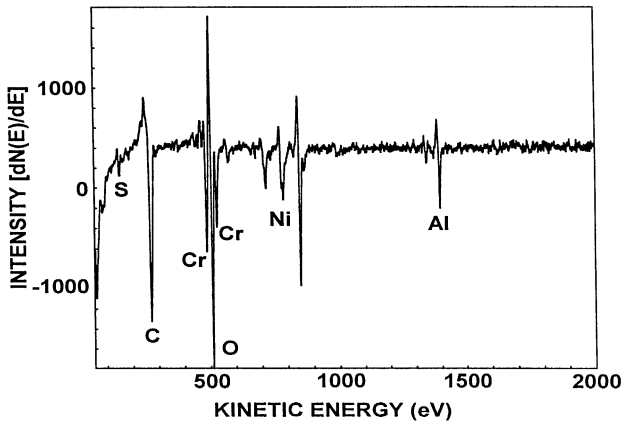

Fig. 4. Example of an AES spectrum showing a differential mode, $dN(E)/dE$, plot of Ni–Cr–Be dental alloy.

improvements in signal-to-noise ratios were achieved by double integration over the Auger structure while maintaining the ability to exactly correct for potential modulation distortions [38].

To date, the most accurate surface analyses with AES have employed elemental sensitivities derived empirically from standard materials of similar chemical matrix to the unknown sample [41]. Such a procedure is complicated by the need for the standard material to have a surface similar to the unknown rather than just a similar bulk chemistry. Many biomaterial surfaces, such as HA, are too complex to characterize in many instances, and analysts have therefore relied on elemental sensitivities derived from elemental standards. However, the accuracy of these quantitative analyses is within 30% of the element when using published elemental sensitivity factors [42]. This high experimental error has resulted in attempts to derive equations for the semi-empirical elemental sensitivity factor [43–46]. Applying the pseudo-first principles corrections scheme to a series of Cr–Fe, Cr–Ni, and Cu–Au alloys, the concentrations of all tested alloys except Cr–Fe have a smaller error than concentrations obtained using sensitivity factors from the Handbook of Auger electron spectroscopy [45]. Other semi-empirical elemental sensitivities such as those derived by Payling were reported to be comparable with experimental relative elemental sensitivities from the Handbook of Auger electron spectroscopy, suggesting that the semi-empirical theory is now capable of providing elemental sensitivities for analysis, in a predictive way, where reliable empirical sensitivities are missing [47]. It should also be noted that the relative sensitivity factors for differential spectra is different from the direct spectra, and that quantitative detection sensitivity for most elements is from 0.1 to 1 at% [48].

3. Applications

Auger electron spectroscopy has been commonly used for analyzing metallic and ceramic biomaterials [5, 49]. Two major techniques used for characterizing biomaterial surfaces are depth profiling and surface composition analyses.

3.1. Depth profiling

The use of AES during depth profiling is a destructive technique using ion sputtering. Sputtering is site dependent with most exposed atoms having the highest sputtering probability. However, the statistical contribution to the depth resolution for depths greater than 10 nm is approximately constant and, depending on the parameters, will probably be in the range 1–2 nm instead of increasing with the square root of depth [50].

During profiling, profile distortions must be taken into account in order to reveal the true original profile. Profile distortions are caused by sputtering-induced topographical and compositional changes of the instantaneous sample surface as well as changes of the electron mean free path. Depth resolution function must be known for the deconvolution of the measured concentration profiles. This resolution function is directly obtained by sputtering through a very thin sandwich layer. However, it must be noted that depth profiling of any surface requires the ion beam to be carefully positioned. The angular distribution of the microplanes making up the rough substrate surface contributes to the loss in resolution. This loss can be significant, even for angular distributions as low as 1 [51]. However, the resolution degradation is the lowest for a sputtering beam aligned along the average surface normal. Thus, careful positioning of the analyzing electron beam is required to minimize resolution loss due to a relatively large surface roughness.

Energetic inert gas ions, such as argon, are often used to sputter the surface [52, 53]. Sputtering is often continuous, and AES is conducted in cycles on a set of selected elemental peaks. The principle advantages of this technique include (a) variable information depth, typically between 0.5 and 3 nm, (b) analyses independent of the sputtering yield, (c) a small influence from the matrix on the elemental sensitivity factor, (d) a small analyzed area as compared to the sputtered area, thereby minimizing crater edge effects (e) lower electron escape depth for low-energy transitions (LVV, MVV and etc.), (f) a smaller data acquisition time, and (g) the possibility of continuous analysis during sputtering [53]. Like most techniques, the main steps of depth profiling involve calibration of the sputtering time scale in terms of the mean eroded depth, and the intensity of the Auger signal must be calibrated in terms of local elemental concentration. Sputtering rate or mean eroded depth of a surface is dependent on many parameters such as energy, yield, mass and angle of incidence of the ions and the instantaneous surface composition [46, 47, 54–56].

The sputtering rate (m/s) of a material is determined by the equation

$$\text{Sputtering rate}(z) = (M/\rho N_A e)\mathrm{S}j_p,$$

where M is the mole mass (kg mole^{-1}), ρ is the density (kg m^{-3}), N_A is the Avogrado number (6.02×10^{26} kg mol), e is the electron charge (1.6×10^{-19} As), S is the sputtering yield (atoms/ion) and j_p is the primary ion current density (A m^{-2}) [53]. However, the sputtering rate obtained from this equation is only an approximation since the sputtering yield (S) on the equation depends on parameters such as energy, mass, angle ion incidence of ions, and instantaneous surface composition [52, 57, 58]. In most instances, where reliable and reproducible thickness measurements are required, the sputtering rate is measured by sputtering a layer of a standard

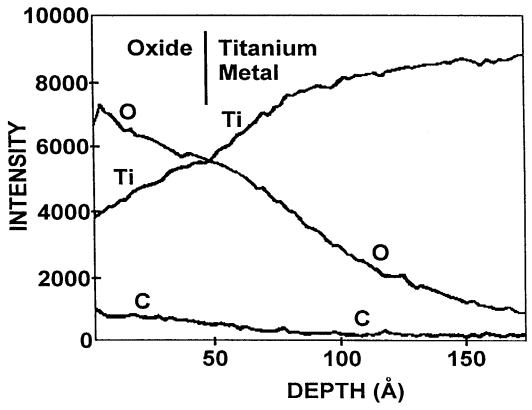

Fig. 5. AES depth profile of passivated titanium. The thickness of the oxide layer is relative to the sputtering rate of Ta_2O_5.

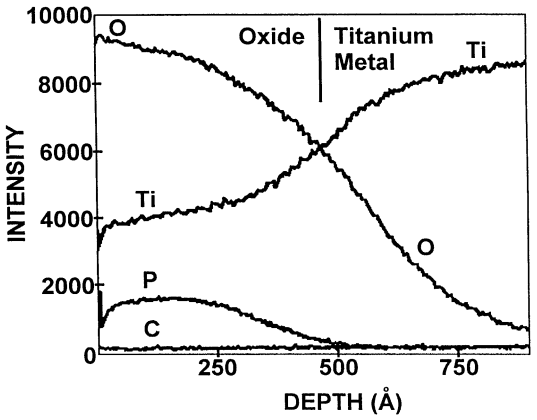

Fig. 6. AES depth profile of anodized titanium. The thickness of the oxide layer is relative to the sputtering rate of Ta_2O_5.

material (usually Ta_2O_5 or Ta) of known thickness for a known period of time. Methods for acquiring a standard layer of known thickness include metallic evaporation and anodization [59–61]. The use of Ta_2O_5 as a reference material has been widely reported [5, 62–64]. The oxide thickness of all surfaces, relative to the sputtering rate of Ta_2O_5, is approximated by multiplying the sputtering rate by the crossover time obtained from the Auger depth profile during continuous sputtering. For a Ti surface, the crossover time is the time corresponding to equal intensities of the Ti and oxygen (O) Auger signals.

The crossover time of Ti and O Auger signals on passivated and anodized Ti surfaces is shown in Figs. 5 and 6. With a 30 take off angle, an accelerating electron beam of 10 keV, a probe energy of 4.7×10^{-7} A, a modulation energy of 5 eV, a probe diameter of 10 μm, and continuous depth profiling using argon ions at approximately 2×10^{-2} Pa (sputtering energy of 3 keV and 3 mA), the passivated and anodized Ti surfaces were found to have an oxide thickness of 41 ± 18 and 436 ± 49, respectively [43].

Auger electron spectroscopy has also been used for analyzing in vitro oxide growth on Ti [4]. After 1 week immersion in a phosphate buffered solution, AES depth profiles indicated as statistical increase in oxide thickness for radiofrequency glow discharged (RFGD) Ti surfaces from 36.8 ± 7.4 Å to 59.4 ± 11.5 Å, an increase of 61.4%. Similarly, the oxide on autoclaved Ti surfaces increased by 53.6% from 45.3 ± 3 Å to 69.6 ± 9.9 Å after 1 week immersion in a phosphate buffered solution. Calcium and phosphorus ions were also found within the oxide for both RFGD or autoclaved surfaces, indicating the diffusion of both ions to the metallic oxide.

As observed in these studies and in other studies, parameters for data collection are critical in preventing misleading results. It has been observed that the length of the alternating sputtering and analysis cycles, ion beam energy, electron beam current density and oxidation composition are found to significantly influence depth profiles. Profile broadening occurs with long analysis cycles coupled with short sputtering cycles or too low ion beam intensities [65]. This effect is probably due to the readsorption/reoxidation at the surface. Ion bombardment of Ti surfaces has a profound effect on surface composition, producing a reduction of the oxide on the Ti surfaces [66]. Depth resolution characterized by the width of the transition region between oxide and metal has been reported to decrease with increasing ion-beam energy and with increasing thickness of the sputtered layer [67]. Other studies have also shown that increasing ion and electron beam energy results in an apparent reduction effect and the formation and buildup of carbide at the sample surface [68]. The mechanisms of carbide buildup probably involves interactions between adsorbed carbon species such as carbon monoxide or hydrocarbons with an activated titanium oxide surface and the impinging electrons [68].

It can be seen from Fig. 7 that with ion bombardment, Ti Auger signals undergo a shape change as a result of alternate sputtering and analysis cycles. The Ti surface exhibits a broad asymmetrical $L_3M_{2,3}M_{4,5}$ transition peak in the 400–425 eV region which is predominantly from valence band transitions. This broad asymmetrical peak corresponds to a TiO_2 spectrum observed by other investigators [69]. With every 10 s of ion bombardment, this band increases and becomes more similar to a Ti metal [69, 70]. This change in the Auger valence band spectra has been related to transitions arising from oxygen 2s and titanium 3d, 4s molecular orbitals. Using a molecular orbital model, differences in spectral shapes have been reported to be linked with differences in the density of state of oxygen-titanium molecular orbitals [69].

Depth profiling can also be used to determine the subsurface composition of biomaterials. In the case of ion

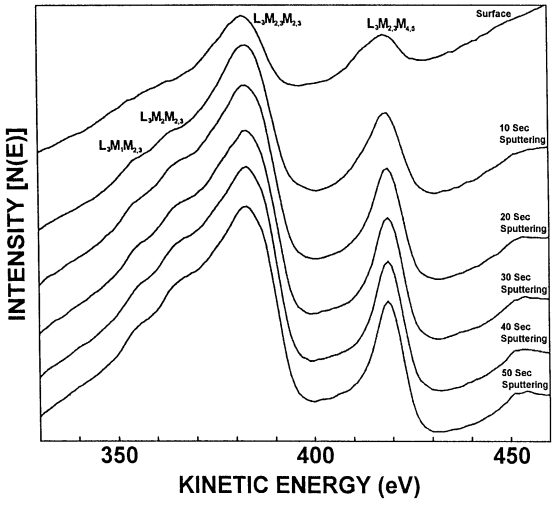

Fig. 7. Ti_{LMM} $N(E)$ spectra of passivated titanium showing shape changes as a result of alternate sputtering and analysis cycles.

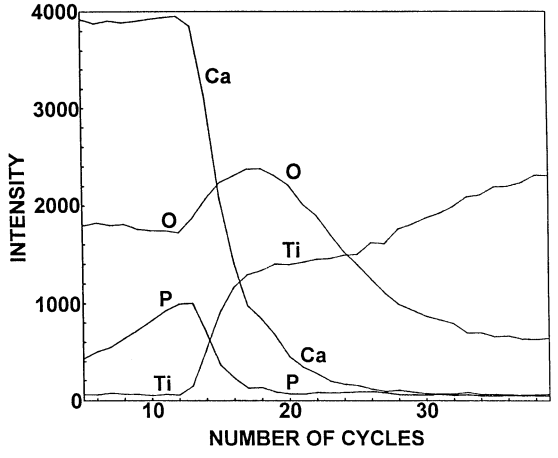

Fig. 8. AES depth profile of HA coatings showing the migration of phosphorus (P) during ion bombardment.

beam sputtered HA coatings on Ti surfaces, diffusion of both calcium (Ca) and phosphorus (P) into the oxide layer has been observed (Fig. 8). This diffusion of Ca and P ions into the oxide layer has also been observed with other analytical methods such as X-ray photoelectron spectroscopy [71]. The coexistence of the coatings within the titanium oxide suggests the occurrence of chemical bonds between the coatings and metallic substrates. Phosphorous can migrate in advance of the Auger signal until the profile reaches the Ti oxide/metal interface. Thus, the diffused P concentration at the oxide/metal interface is higher than the outermost oxide surface. This P-rich region have been formed by a rapid reaction of the P at the oxide surface, followed by diffusion of the P through the oxide, with a final reaction at the metallic surface [72]. In another study, an additional peak at 116.5 eV was observed during argon ion bombardment

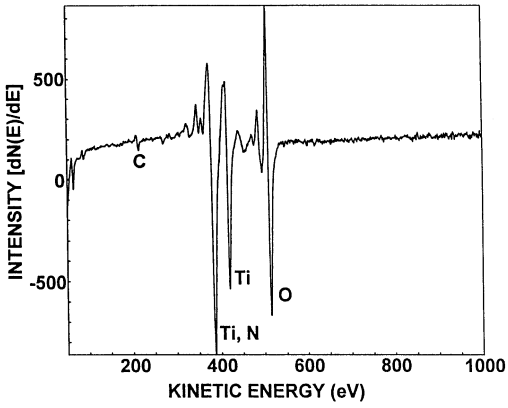

Fig. 9. Ti Auger derivative surface spectrum of passivated titanium showing a small carbide peak after minimal beam exposure.

of sputtered HA surfaces [49]. Similar to the reduction of Ti oxide during ion bombardment, the formation of this peak at 116.5 is thought to be either by a reduction reaction of the phosphate group by a preferential sputtering of O, thereby resulting in an enrichment of free P at the analyzed area.

3.2. Chemical information

Auger spectra can also provide local chemical information. However, it has been reported that the length of the analysis period significantly influences carbide buildup on biomaterial surfaces. Since metallic Ti is a very strong reducing agent, its surface is prone to carbide buildup. In Figs. 9 and 10, a buildup of the carbide peak is shown after long beam exposure whereas a significantly reduced carbide peak is shown with minimal beam exposure. Carbide formation can affect the relative peak-to-peak intensities of the oxygen and titanium Auger signals, and thus interfere with the determination of oxide stoichiometry [67]. In another study, an adsorbed monolayer of carbon monoxide on tungsten, molybdenum, niobium, and tantalum surfaces resulted in a shift of 0.5 to 1.0 eV to a lower energy [68]. This shift was attributed to the electron transfer from the metal to the adsorbed monolayer of carbon monoxide. Other factors that could interfere with the analysis of oxide stoichiometry include film thickness [67]. Films less than 100 Å thick may be sputtered away before steady-state sputtering is achieved. It is known that preferential sputtering exists and thus sputter profiling of films less than 100 Å do not provide an absolute quantitative composition [67, 71, 73]. Instead, the composition of the altered surface layer is often reported [67].

Numerous investigations on possible beam effects have been performed [65–67, 74]. It has been observed that the Ti $L_{2,3}M_{2,3}V$ peak consists of a double structure with peaks at approximately 418 and 421 eV, respectively.

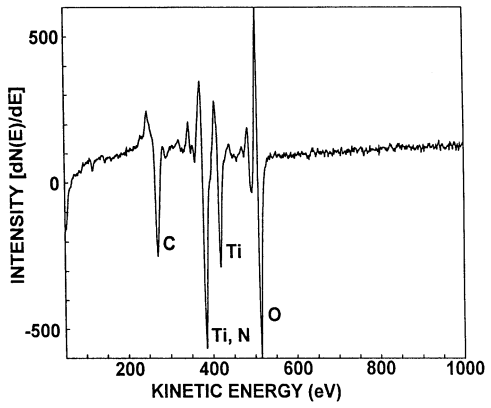

Fig. 10. Ti Auger derivative surface spectrum of passivated titanium showing a significant carbide buildup after long beam exposure. Overlap of the Ti and N peaks were also observed.

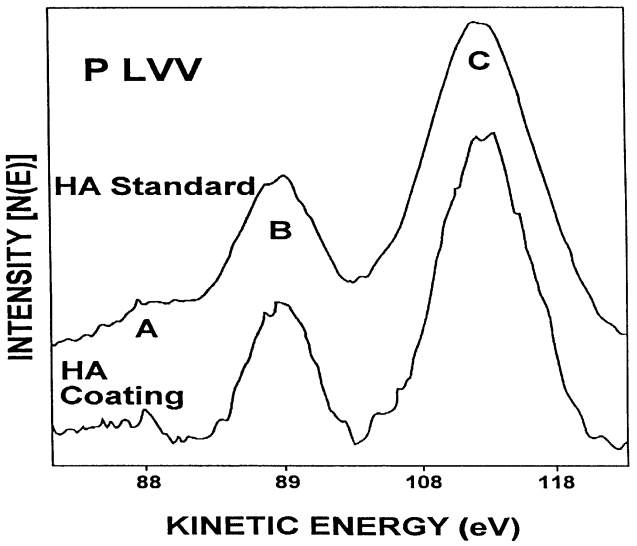

Fig. 11. PLVV $N(E)$ surface spectra of HA standard and HA coatings. The kinetic energies A, B, and C correspond to the energies in Table 1.

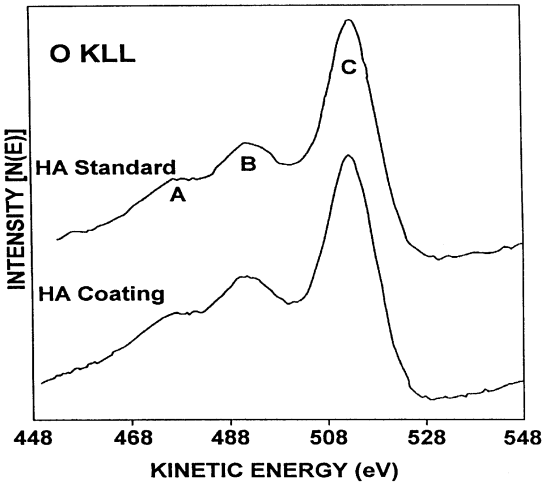

Fig. 12. OKLL $N(E)$ surface spectra of HA standard and HA coatings. The kinetic energies, A, B, and C correspond to the energies in Table 1.

The relative heights of these peaks can be used as 'finger prints' of TiO_2 surfaces which have undergone different degrees of reduction. At current densities less than 1 mA/cm^2, no significant changes in the Ti LMV peak have been reported, whereas gradual increases in current density have resulted in increasing height of the 421 eV peak [65].

Problems in providing chemical information arise when peaks for major elements overlap. This overlapping has been observed on nitric acid passivated Ti surfaces and Ti nitrided surfaces (Figs. 9 and 10). The detection of nitrogen (N) on Ti surfaces is not easily accomplished using AES due to the overlapping of the N KL_2L_2 (384 eV), N KL_2L_3 (392 ev) and Ti $L_3M_{23}M_{23}$ peaks (383, 388 eV). This masking of N peaks by Ti peaks during AES analysis has been commonly observed by investigators [64, 65, 75]. As reported in other studies, depth profiling of TiN surfaces has been shown to be very problematic, due to the overlapping of the N KL_2L_2, N KL_2L_3 and Ti $L_3M_{23}M_{23}$ peaks [75]. Thus, during a peak-to-peak height measurement for routine depth profiling analysis of TiN surfaces or any surfaces having overlapping of major transition peaks, a multiple technique approach must be used when interpreting data.

Chemical bonding effects are also reflected in both the shapes and intensities of Auger peaks, which are very sensitive to adsorbates. The core-valence–valence (CVV) Auger lines exhibit maximum changes due to changes in chemical environment. Figs. 11 and 12 show no significant differences in the Auger spectra of the HA standard and ion beam sputtered HA coatings. As shown in Table 1, the kinetic energies of P Auger (LVV) peaks change from a phosphide to a phosphate. This change is kinetic energy of the P Auger peaks occurs due to a change in the P 3p level which undergoes a chemical shift to a higher binding energy. The shape of the observed P LVV peaks reveals that they are associated with strong P–O bonds [76]. The O KLL Auger lines are identical in shape to

Table 1
Auger kinetic energies ($\pm$1 ev) for HA standard and HA coatings

Samples	Peaks	P LVV	O KLL
HA standard			
	A	87	472
	B	97	489
	C	112	511
HA coatings			
	A	88	473
	B	97	490
	C	112	512

those observed in bulk oxides [77]. The 15 eV separation observed between the two principal phosphorous peaks, B and C in Fig. 11, is in excellent agreement with the principal Auger peaks observed and calculated for the Li_3PO_4, which is an ionic material. In other words, using AES, the chemical composition of the sputtered HA coatings is similar to the HA standard. In combination with other analytical analyses such as X-ray diffraction, Fourier transform infrared spectroscopy and X-ray photoelectron spectroscopy, the sputtered HA coatings was concluded to have chemical and structural properties similar to HA [12, 71, 78–80].

4. Summary

Analysis of the surface composition of biomaterials is critically needed to better understand the interactions between the host and implant. Among the many surface analytical tools, AES has been shown to be very effective for surface composition analysis, with ability to detect all elements except hydrogen and helium. Depth-compositional profiling and thin-film analysis can also be conducted with AES. However, it should be remembered that electron beam damage can severely limit useful analysis of organic and biological material and occasionally ceramic materials. Electron beam charging may limit analysis when examining highly insulating materials. Carbide buildup during long beam exposure can affect the relative peak-to-peak intensities of the oxygen and metal Auger signals, thereby interfering with the determination of oxide stoichiometry. In addition, the accuracy of quantitative analyses is limited to the availability of standards ($\pm 30\%$ of the element when using published elemental sensitivity factors). Semi-empirical elemental sensitivities, comparable to the Handbook of Auger electron spectroscopy, have been developed, suggesting that the semi-empirical theory is capable of providing reliable elemental sensitivities where reliable empirical sensitivities are missing. Although AES can be powerful tool for the characterization of biomaterial surfaces, the operator must be aware of its limitations. In summary, AES when used with other techniques such as X-ray diffraction, X-ray photoelectron spectroscopy, Fourier transform infrared spectroscopy, and Raman spectroscopy can contribute valuable data required to fully characterize biomaterials surfaces.

References

[1] Kasemo B, Lausmaa J. Surface science aspects on inoraganic biomaterials. CRC Crit Rev Biocomp 1986;2:335–80.
[2] Mattox DM. Adhesion and surface preparation. In: Bunshah, editor. Deposition technologies for films and coatings: developments and applications. NJ: Noyes Publications, 1982:63–82.
[3] Baier RE. Improved passivation of implantable biomaterials by glow-discharged processes. Surfaces in biomaterials symposium, Minneapolis, 1991.
[4] Kawahara D, Ong JL, Raikar GN, Lucas LC, Lemons JE, Nakamura M. Surface characterization of radio-frequency glow-discharged and autoclaved titanium before and after simulated biological fluid exposure. Inter J Oral Maxillolfac Impl 1996; 11:435–42.
[5] Keller JC, Draughn RA, Wightman JP, Dougherty WJ, Meletious SD. Characterization of sterilized cp titanium implant surfaces. Inter J Oral Maxillolfac Impl 1990;5:360–67.
[6] Doundoulakis JH. Surface analysis of titanium after sterilization: role in implant tissue interface and bioadhesion. J Prosthet Dent 1987;58:471–8.
[7] Olsson J, Carlen A, Holmberg K. Inhibition of Streptococcus mutans adherence by means of surface hydrophilization. J Dent Res 1990;69:1586–91.
[8] Olsson J, Carlen A, Holmberg K. Surface modification of hydroxyapatite to avoid bacterial adhesion. Col Polym Sci 1991; 269:1295–302.
[9] Hench LL, Paschall HA. Histochemical responses at a biomaterial's interface. J Biomed Mater Res 1974;8:49–64.
[10] Jarcho M, Kay JF, Gumaer KI, Doremus RH, Drobeck HP. Tissue, cellular and subcellular events at a bone-ceramic hydroxylapatite interface. J Bioengng 1977;1:79–92.
[11] Ong JL, Lucas LC, Raikar GN, Connatser R, Gregory JC. Spectroscopic characterization of passivated titanium in a physiologic solution. J Mater Sci: Mater Med 1995;6:113–9.
[12] Ong JL, Lucas LC, Raikar GN, Weimer JJ, Gregory JC. Surface characterization of ion-beam sputter-deposited Ca-P coatings after in vitro immersion. Col and Surf 1994;87:151–62.
[13] Hanawa T, Ota M. Calcium phosphate naturally formed on titanium in electrolyte solution. Biomaterials 1991;12:767–73.
[14] Tengvall P, Lundström I. Physico-chemical considerations of titanium as a biomaterial. Clin Mater 1992;11:115–34.
[15] Driessens FCM, van Dijk JWE, Borggreven JMPM. Biological calcium phosphates and their role in the physiological of bone and dental tissue. I. Composition and solubility of calcium phosphates. Calcif Tiss Res 1987;26:127–37.
[16] Okazaki M. F-Co_3^{2-} interaction in IR spectra of fluoridated CO_3-apatites. Calcif Tiss Int 1983;35:78–81.
[17] Ong JL, Chittur KK, Lucas LC. Dissolution/reprecipitation and protein adsorption studies of calcium phosphate coatings by FT-IR/ATR techniques. J Biomed Mater Res 1994; 28:1337–46.
[18] LeGeros RZ. Formation of calcium phosphates in vitro. In: Myers HM, editor. Calcium phosphates in oral biology and medicine. New York: Karger, 1991:46–67.
[19] Jung A, Bisaz S, Fleisch H. The binding of pyrophosphate and two diphosphonates by hydroxyapatite. Calc Tiss Res 1973; 11:269–80.
[20] Bartels T, Arends J. Adsorption of a polyphosphonate on bovine enamel and hydroxyapatite. Caries Res 1979;13:218–26.
[21] Horbett TA. Protein adsorption on biomaterials. In: Cooper SL, Peppas NA, editors. Biomaterials: interfacial phenomena and applications, advances in chemistry series, vol. 199. Washington DC: American Chemical Society, 1982:233–44.
[22] Albrektsson T, Branemark PI, Hansson HA, Lindstrom J. Osseointegrated titanium implants. Requirements for ensuring a long-lasting direct bone-to-implant anchorage in man. Acta Orthop Scand 1981;52:155–70.
[23] Michaels CM, Keller JC, Stanford CM. In vitro periodontal ligament fibroblast attachment to plasma cleaned Ti surfaces. J Oral Implant 1991;17:132–39.
[24] Keller JC, Dougherty WMJ, Grotendorst GR, Wightman JP. In vitro cell attachment to characterized cp Ti surfaces. J Adhesion 1989;28:115–33.

[25] Hanein D, Sabanay H, Addadi L, Geiger B. Selective interactions of cells with crystal surfaces: implications for the mechanism of cell adhesion. J Cell Sci 1993;104:275–88.
[26] Ricci JL, Spivak JM, Blumenthal NC, Alexander H. Modulation of bone ingrowth by surface chemistry and roughness. In: Davies JE, editor. The bone and biomaterials interface. Toronto: University of Toronto Press, 1991:205–13.
[27] Hercules DM. Surface analysis: an overview. Crit Rev Surf Chem 1992;1:243–77.
[28] Lander JJ. Auger peaks in the energy spectra of secondary electrons from various materials. Phys Rev 1953;91:1382–87.
[29] Harris LA. Analysis of materials by electron-excited Auger electrons. J Appl Phys 1968;39:1419–27.
[30] Harris LA. Some observations of surface segregation by Auger electron emission. J Appl Phys 1968;39:428–31.
[31] Bumgardner JD, Lucas LC. Surface analysis of nickel-chromium dental alloys. Dental Mater 1993;9:252–9.
[32] Miller RG, Bowles CQ, Eick JD, Gutshall PL. Auger electron spectroscopy of dentin: elemental quantification and the effects of electron and ion bombardment. Dent Mater 1993;9:280–5.
[33] Koopman MC, Thompson RG. Interface segregation in a nickel base superalloy. Microbeam Analysis 1990;25:263–4.
[34] Palmberg PW, Bohn GK, Tracy JC. High sensitivity Auger electron spectrometer. Appl Phys Lett 1969;15:254–5.
[35] Nordling C, Siegbahn K. New precision spectroscopy of atoms and molecules. Rev Roumaine Phys 1966;11:797–818.
[36] Nordbery N, Albridge RC, Bergmark T, Ericson U, Hedman J, Nordling C, Siegbahn K, Lindberg BJ. Molecular spectroscopy by means of electron spectroscopy for chemical analysis. Charge distribution in nitrogen compounds. Ark Kemi 1967;28:257–78.
[37] Rivière JC. Instrumentation. In: Briggs B, Seah MP, editors. Practical surface analysis, 2nd ed., vol. 1. New York: Wiley, 1990: 19–83.
[38] Grant JT, Haas TW, Houston JE. The effect of modulation amplitude on electron-excited Auger data from titanium. Surf Sci 1974;42:1–11.
[39] Grant JT, Haas TW, Houston JE. Quantitative Auger analysis using integration techniques. Phys Lett 1973;45A:309–10.
[40] Grant JT, Haas TW, Houston JE. Quantitative comparison of titanium and titanium monoxide surfaces using Auger electron and soft X-ray appearance potential spectroscopies. J Vac Sci Technol 1974;11:227–30.
[41] Mitchell DF, Sproule GI, Graham MJ. Quantitative analysis of iron oxides using Auger electron spectroscopy combined with ion sputtering. J Vac Sci Technol 1981;18:690–4.
[42] Davis LE, MacDonald NC, Palmberg PW, Riach GE, Weber RE. In: Handbook of Auger electron spectroscopy. 2nd ed. Eden Prairie: Physical Electronics Industries.
[43] Hall PM, Morabito JM. Matrix effects in quantitative Auger analysis of dilute alloys. Surf Sci 1979;83:391–405.
[44] Payling R. Modified elemental sensitivity factors for Auger electron spectroscopy. J Electron Spectrosc Relat Phenom 1985; 33:99–104.
[45] Mroczkowski S, Lichtman D. Quantitative AES of binary alloys: comparison between handbook and pseudo-first principles corrections. Surf Sci 1983;127:119–34.
[46] Ferron J, De Bernardez LS, Buitrago RH. Comments on 'pseudo first principles' calculations of Auger sensitivity factors. Surf Sci 1984;145:L501–3.
[47] Payling R. Semi-empherical elemental sensitivities for quantitative Auger electron spectroscopic analysis. J Electron Spectrosc Relat Phenom 1985;37:225–39.
[48] Seah MP. A review of the analysis of surfaces and thin films by AES and XPS. Vaccum 1984;34:463–78.
[49] Raemdonck WV, Ducheyne P, De Meester P. Auger electron spectroscopic analysis of hydroxylapatite coatings on titanium. J Am Ceramic Soc 1984;67:381–4.
[50] Seah MP, Sanz JM, Hofmann S. The statistical sputtering contribution to resolution in concentration-depth profiles. Thin Solid Films 1981;81:239–46.
[51] Seah MP, Lea C. Depth resolution in composition profiles by ion sputtering and surface analysis for single-layer and multilayer structures on real substrates. Thin Solid Films 1981;81: 257–70.
[52] Seah MP. Pure element sputtering yields using 500–1000 eV argon ions. Thin Solid Films 1981;81:279–87.
[53] Hofmann S. Depth profiling in AES and XPS. In: Briggs D, Seah MP, editors. Practical surface analysis, 2nd ed., vol. 1, Auger and X-ray photoelectron spectroscopy. New York: Wiley, 1990: 143–255.
[54] Mroczkowski S, Lichtman D. Reply to Comments on pseudo-first principles calculations of Auger sensitivity factors. Surf Sci 1985;154:L221–4.
[55] Mroczkowski S, Lichtman D. Calculated Auger yields and sensitivity factors for KLL-NOO transitions with 1–10 kV primary beams. J Vac Sci Technol 1985;A3:1860–5.
[56] Payling R, Szajman J. On the semi-empherical elemental sensitivity factors for AES: ionization cross-section and electron mean free path. J Electron Spectrosc Relat Phenom 1987;43: 37–51.
[57] Oechsner H. Sputtering—a review of some recent experimental and theoretical aspects. Appl Phys 1975;8:185–98.
[58] Coburn JW. Sputtering in the surface analysis of solids: a discussion of some problems. J Vac Sci Technol 1976;13:1037–44.
[59] Sato T, Nagasawa T, Sekine T, Sakai Y, Buonaquisti AD. Conversion of Auger sensitivities at one primary excitation energy to those at another. Surf Interface Anal 1989;14:787–93.
[60] Holloway PH, Holloway DM. The effect of electromagnetic fields on Auger electron peak-height ratios. Surf Sci 1977;66: 636–40.
[61] Sickafus EN, Holloway DM. Specimen position effects on energy shifts and signal intensity in a single-stage cylindrical-mirror analyzer. Surf Sci 1975;51:131–9.
[62] Fine J, Navinsek B. An NBS standard reference material for depth profile analysis. Surf Interfacial Anal 1988;11:542–3.
[63] Seah MP, Holbourn MW, Ortega C, Davies JA. An intercomparison of tantalum pentoxide reference studies. Nucl Inst Meth Phys Res 1988;B30:128–39.
[64] Ong JL, Lucas LC, Raikar GN, Gregory JC. Electrochemical corrosion analyses and characterization of surface-modified titanium. Appl Surf Sci 1993;72:7–13.
[65] Lausmaa J, Kasemo B. Surface spectroscopic characterization of titanium implant materials. Appl Surf Sci 1990;44:133–46.
[66] Thomas S. AES-ion sputtering analysis and the surface composition of TiO_2. Surf Sci 1976;55:754–8.
[67] Mathieu HJ, Mathieu JB, McClure DE, Landolt D. Beam effects in Auger electron spectroscopy analysis of titanium oxide films. J Vac Sci Technol 1977;14:1023–8.
[68] Haas TW, Grant JT, Dooley III GJ. Identification of the chemical state of adsorbed species with Auger electron spectroscopy. In: Ricca F, editor. Adsorption-desorption phenomena. New York: Academic Press, 1972:359–68.
[69] Solomon JS, Baun WL. Molecular orbital effects on the Ti LMV Auger spectra of TiO and TiO_2. Surf Sci 1975;51:228–36.
[70] Bassett PJ, Gallon TE. The effect of oxidation on the high resolution Auger spectrum of titanium. J Electron Spectrosc Relat Phenom 1973;2:101–4.
[71] Ong JL, Harris LA, Lucas LC, Lacefield WR, Rigney D. X-ray photoelectron spectroscopy characterization of ion-beam sputter-deposited calcium phosphate coatings. J Am Ceram Soc 1991; 74:2301–4.
[72] Chang CC, Adams AC, Quintana, Sheng TT. Phosphorus concentration profiles in P-doped silicon dioxide measured using Auger spectroscopy. J Appl Physics 1974;45:252–6.

[73] Tarng ML, Wehner GK. Alloy sputtering studies with in situ Auger electron spectroscopy. J Appl Phys 1971;42:2449–52.
[74] Davis GD, Natan M, Anderson KA. Study of titanium oxides using Auger line shapes. Appl Surf Sci 1983;15:321–33.
[75] Pantel R, Levy D, Nicolas D. Auger electron spectroscopy technique for nitrogen depth profiling in titanium compounds. J Vac Sci Technol 1988;A6:2953–6.
[76] Bernett MK, Murday JS, Turner NH. An interpretation of the Auger LVV transitions from oxides of third-row elements. J Electron Spectrosc Relat Phenom 1977;12:375–93.
[77] Wagner CD, Zatko DA, Raymond RH. Two-dimensional chemical state plots: A standardized data set for use in identifying chemical states by X-ray photoelectron spectroscopy. Anal Chem 1980;52:1445–51.
[78] Ong JL, Lucas LC, Lacefield WR, Rigney ED. Structure, solubility and bond strength of thin calcium phosphate coatings produced by ion beam sputter deposition. Biomaterials 1992; 13:249–4.
[79] Ong JL, Lucas LC. Post-deposition heat treatments for ion beam sputter deposited calcium phosphate coatings. Biomaterials 1994; 15:337–41.
[80] Lucas LC, Lacefield WR, Ong JL, Whitehead. Calcium phosphate coatings for medical and dental implants. Coll Surf 1993; 77:141–7.